Available online at www.sciencedirect.com
SCIENCE DIRECT®
Journal of Chromatography A, 1048 (2004) 161–172
JOURNAL OF CHROMATOGRAPHY A
www.elsevier.com/locate/chroma

Effect of hindered diffusion on the adsorption of proteins in agarose gel using a pore model

Jan Gutenwik, Bernt Nilsson, Anders Axelsson*

Department of Chemical Engineering, Lund University, P.O. Box 124, SE-221 00 Lund, Sweden

Received 5 January 2004; received in revised form 26 July 2004; accepted 26 July 2004

Abstract

The hindered diffusion and binding of proteins of different sizes (lysozyme, BSA and IgG) in an agarose gel is described using adsorption kinetic and diffusional data together with an experimentally determined pore size distribution in the gel. The validity of the pore model, including variable diffusion coefficients and porosities is tested against experimental confocal microscopy data. No fitting parameters were used in the present model. The importance of knowing the gel structure is demonstrated especially for large proteins such as IgG. Experimental confocal microscopy data can be explained by the present model.

Keywords: Hindered diffusion; Proteins; Pore size distribution; Confocal microscopy

1. Introduction

This work deals with a phenomenon usually called hindered or restricted diffusion. In this process, the diffusing molecules are hindered not only by other molecules but also by physical hindrances created, for example, by a polymer network. This forces the molecules to become buoyant around obstacles, increasing the time required for the diffusive mass transfer. Hindered diffusion is important in many, completely different, kinds of systems, for example:

- diffusion and reaction within an immobilized cell preparation [1],
- diffusion and adsorption of proteins in chromatography gels,
- diffusion through polymer networks in controlled-release pharmaceuticals [2,3].

It is the second of these systems that is discussed in detail in this work.

Chromatography is the technique most widely used to purify proteins. To fully understand and to predict the performance of the purification process detailed knowledge of the adsorption kinetics and the diffusive behavior is required. In this work, an intrinsic model describing the diffusive process and the adsorption within the porous network of porous gel beads is presented.

One of the most commonly used chromatography support matrices is agarose gel in the form of beads. This is due to its great chemical stability, the hydrophilic environment and the open structure, facilitating the transport of protein molecules through the gel network. However, although it has large pores, there is still a decrease in diffusivity inside these agarose beads compared to free diffusion in liquid, especially for large molecules. Furthermore, the adsorption of the protein molecules onto the gel polymer network decreases the space available for the remaining diffusing protein molecules. This effect becomes gradually more severe as the adsorption process proceeds, and is accentuated when the diameter of the protein molecule is close to the diameter of the pore. Therefore, the pore size distribution of the gel beads is important in determining the diffusive characteristics of the proteins. In this work an experimentally obtained pore size distribution was used. The structure of agarose has been thoroughly investigated by Medin [4] who measured the pore size distribution and found it to be bimodal. Loh and Wang [5] have studied

* Corresponding author. Tel.: +46 46 2228287; fax: +46 46 2224526.
E-mail address: anders.axelsson@chemeng.lth.se (A. Axelsson).

0021-9673/$ – see front matter © 2004 Elsevier B.V. All rights reserved.
doi:10.1016/j.chroma.2004.07.052

pore size distributions using mercury intrusion experiments and found similar results for other porous media. Chiang et al. [6] compared different pore size distributions for enzyme loading. Li et al. [7] calculated average pore diameters for agarose and alginate gels, giving an average pore diameter in good agreement with the data of Medin. Li et al. [7] also studied how the degree of cross-linking affected diffusion.

Several others have used pore network models to describe diffusion in heterogeneous media. McCoy and Liapis [8] developed a model describing the adsorption of adsorbate onto ligands on porous and non-porous particles in column systems. They took into account the adsorption, and the adsorbing molecules occupying pore area, but did not consider the decrease in effective pore volume. Thus, their effective pore radius does not decrease. However, their diffusion coefficient decreases with the amount of molecules bound to the ligands. In our model, the effective pore volume decreases due to the binding of molecules to the ligands. The rate of diffusion thus varies with time and position in the pores. Clark et al. [9] described a decrease in pore radius when an enzyme is attached to the pore surface. The use of connectivity models [10–15] is often based on theoretical assumptions of the number and frequency of connections between pores. Thus, the degree of connectivity will be more or less a fitting parameter to adjust the model to experiments. Zhang and Seaton [16] have developed a model describing the effective diffusion near the percolation threshold. In the very open hydrogels employed in this work the interconnectivity is very high. Using a percolation model Reyes and Jensen [17] demonstrate how the connectivity causes the accessible porosity to decrease. The effect is most pronounced at low porosities, below about 0.4. On the other hand, the simple pore models should be treated with caution when you are close to the percolation threshold. Still, it is of great value to use simple models to eventually catch the important physical characteristics of a process. Although this present model has a simple physical description (Fig. 1) it includes a variable diffusion coefficient and a variable porosity, it considers a dynamic adsorption–desorption process and it describes the wall effect for the diffusing protein molecules. In this way, it is possible to study and understand the effect of hindered diffusion on the adsorption process in a fairly simple way.

In this paper, we describe the binding of proteins of different sizes in an agarose gel using realistic adsorption kinetic and diffusional data together with an experimentally determined pore size distribution in the gel. The aim is to study the coupled effects of hindered diffusion and adsorption kinetics in a porous gel, describing the gel with a pore model and a given pore size distribution. The model is thus based on our own and others experimental data and commonly adopted knowledge using no fitting parameters to adjust the model to experiments. The validity of the model is tested against experimental confocal microscopy data.

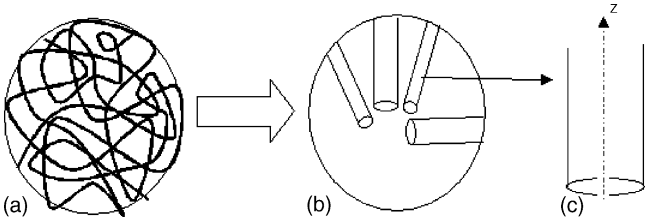

Fig. 1. Simplification of the complex agarose network (a) to a capillary pore distribution model (b) to a single pore model (c).

2. Theory

2.1. Continuity equation for a protein in cylindrical pore [18–21]

$$\frac{\partial C_A}{\partial t} = D\left(\frac{1}{r}\frac{\partial}{\partial r}\left(r\frac{\partial C_A}{\partial r}\right) + \frac{1}{r^2}\frac{\partial^2 C_A}{\partial \theta^2} + \frac{\partial^2 C_A}{\partial z^2}\right) + r_A \quad (1)$$

There is no convection inside the pores in the bead. Diffusion is only studied in the z-direction, i.e. in the direction along the pore (Fig. 1c):

$$\frac{\partial C_A}{\partial t} = D\left(\frac{\partial^2 C_A}{\partial z^2}\right) + r_A \quad (2)$$

D is the pore diffusion coefficient, which decreases during the adsorption process, as described below. This equation is however only valid for a constant diffusion coefficient. The final model presented in this paper considers a variable diffusion coefficient. This is discussed and presented in section 2.2–2.4 and an extended continuity equation is given as Eq. (25). Each pore requires two boundary conditions, one at the inlet and the other at the outlet.

At the inlet, $z = 0$:

$$D\frac{\partial C_A}{\partial z} = -K_{mass}(C_{A_{in}} - C_{A_{boundary}}) \quad (3)$$

Here, K_{mass} is the mass transfer coefficient, $C_{A_{in}}$ is the concentration outside the pore and $C_{A_{boundary}}$ is the concentration at the entrance of the pore.

At the outlet, $z = L$:

$$D\frac{\partial C_A}{\partial z} = 0 \quad (4)$$

This boundary condition is used since all pores lead from the surface to the middle of the bead where it is reasonable to assume that the flux is zero due to the symmetry of the bead.

2.1.1. External mass transfer coefficient

The mass transfer coefficient, K_{mass}, describes the mass transfer rate through the external stagnant boundary layer. The mass transfer is very much dependent on the type of flow outside the bead, which is described by the Reynolds number, Re:

$$Re = \frac{\rho V_{sup} d_p}{\mu} \quad (5)$$

where ρ is the density of the liquid and V_{sup} is the superficial velocity of the bulk flow in a chromatography bed. d_p is the diameter of the bead and μ is the dynamic viscosity.

The Schmidt number, *Sc*, is the quotient between the viscous diffusivity, μ/ρ (m^2/s), and the mass diffusivity of the fluid, D_0 (m^2/s).

$$Sc = \frac{\mu}{\rho D_0} \tag{6}$$

The mass transfer properties are given by the Sherwood number, *Sh*, which is defined by:

$$Sh = \frac{K_{mass} d_p}{D_0} \tag{7}$$

for flow in a packed bed.

$$Sh = 2 + 1.45 Re 1/2 Sc^{1/3} \tag{8}$$

From Eq. (8) it is obvious that the minimum value of *Sh* is 2, which is obtained at no flow or creeping flow conditions. Thus, the mass transfer coefficient, K_S, can be derived from Eq. (7):

$$K_{mass} = \frac{D_0 Sh}{d_p} \tag{9}$$

2.2. Diffusion

2.2.1. Diffusion coefficient for proteins

The diffusivity of solutes in dilute solutions can be estimated from the Stokes–Einstein equation [18,20,22]:

$$D_0 = \frac{RT}{6\pi\mu R_0 A_V} = \frac{k_B T}{6\pi\mu R_0} \tag{10}$$

This gives an estimate of the diffusion coefficient based on the Stokes radius, R_0, and temperature, *T*. Using the Stokes radius as an approximation of the molecular radius gives the following equation [22]:

$$R_0 = \left(\frac{3MW}{4\pi\rho A_V}\right)^{1/3} \tag{11}$$

where MW is the molecular weight of the molecule and ρ is the density of the molecule. The radii and diffusion coefficients of the three protein molecules studied: lysozyme, BSA and IgG are presented in Table 1.

Table 1
Physical data for lysozyme, BSA and IgG

Protein	Molecular weight, MW (g/mol)	Stokes' radius, R_0[a] (nm)	Diffusivity, D_0[b] (m^2/s)
Lysozyme	14800	1.8	1.2×10^{-10}
BSA	66000	3.0	7.1×10^{-11}
IgG	160000	4.0	5.3×10^{-11}

[a] Calculated from Eq. (11).
[b] Calculated from Eq. (10).

2.2.2. Variable pore diffusion coefficient

Various models are presented in the literature describing how the pore diffusion coefficient, *D*, varies with the effective radius of the pores, *r*, and the radius of the diffusing molecule, R_0. *D* is related to the diffusion coefficient in pure water, D_0, and is normally expressed as a function of the quotient, λ, between the molecule radius and the pore radius ($\lambda = R_0/r$) [20,23].

$$\frac{D}{D_0} = 1 + \tfrac{9}{8}\lambda \ln\lambda - 1.54\lambda + O(\lambda^2) \tag{12}$$

$O(\lambda^2)$ is the error, which is normally disregarded for higher orders of λ [20].

Another function describing the variation in the diffusion is the Renkin equation [7,24,25]:

$$\frac{D}{D_0} = (1-\lambda)^2(1 - 2.104\lambda + 2.09\lambda^3 - 0.956\lambda^5) \tag{13}$$

The Ogston theory is also frequently cited. This describes the ratio between the free solution diffusivity and the diffusion through the inlet of a pore [25–31]:

$$\frac{D_e}{D_0} = e^{-\varphi^{0.5}(1+\lambda)} \tag{14}$$

Here, φ is the polymer volume fraction. Since the Ogston theory also takes into account the polymer fraction, this is not a true pore diffusion coefficient, but instead an effective diffusion coefficient.

Another frequently used theory is the Ferry–Faxén equation [32,33]. This is often used in membrane technology, and describes the retention of large molecules in cylindrical pores in membranes.

$$\frac{D}{D_0} = (1-\lambda)^2(1 - 0.104\lambda - 5.21\lambda^2 + 4.19\lambda^3 + 4.18\lambda^4 - 3.04\lambda^5) \tag{15}$$

The four models mentioned above are illustrated in Fig. 2. They are of course only valid for molecules smaller than the pores. The model presented by Cussler is not valid when the size of the pore is only slightly larger than the molecule, as can be seen in Fig. 2. There is a discrepancy between the theory of Ogston and the other theories. This is due to the fact that the Ogston theory considers the polymer content of the gel, thereby further reducing the diffusion coefficient.

Since all these models show the same behavior, only the Renkin model was used in our simulations. Since the effective pore radius decreases, due to molecules binding to the ligands, the pore diffusion coefficient will also decrease with time. This can be seen in Fig. 3, which was obtained by simulation of the model using the base case parameters given in Table 2.

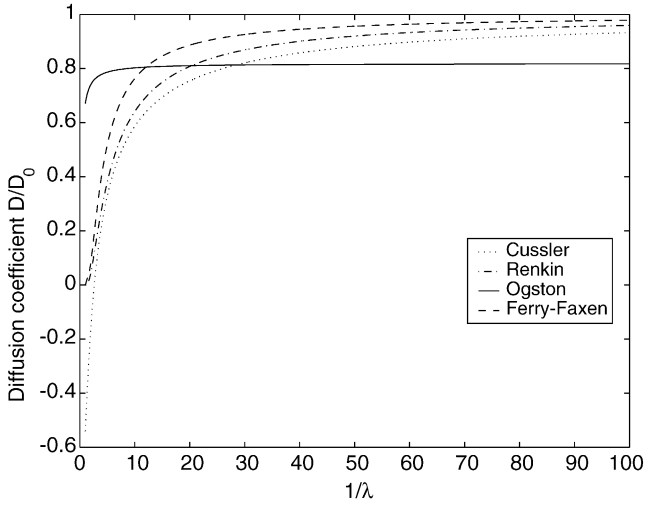

Fig. 2. Diffusion coefficient as a function of pore–molecule ratio, 1/λ.

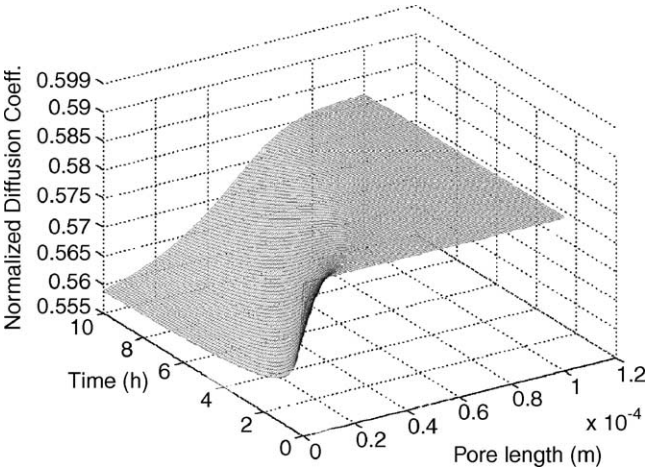

Fig. 3. Diffusion coefficient as a function of time and position in pore. Lysozyme in a pore with radius 15 nm. Parameters given in Table 2 were used.

Table 2
Base case parameters used in the simulations

C_{Ain} (mol/m^3)	7.14×10^{-3}
k_{ads} lysozyme (m^3/(mol s))	1.144
k_{ads} IgG (m^3/(mol s))	5.72
k_{des} lysozyme (s^{-1})	2.0×10^{-3}
k_{des} IgG (s^{-1})	1.0×10^{-2}
K_{mass} (m/s)	6.9×10^{-6}
L (m)	1×10^{-4}
q_{max} lysozyme (mol/(m^3 sedimented gel))	1
q_{max} IgG (mol/(m^3 sedimented gel))	0.0977
R_{pore} (m)	15×10^{-9}
T (K)	293
ε_{bead}	0.75
ε_{bed}	0.37
μ (Pa s)	1005×10^{-6}

Protein data according to Table 1.

2.3. Binding of molecules

2.3.1. Adsorption kinetics

The protein molecules can adsorb onto the ligands inside the pore which, in the present case, is modeled with Langmuir kinetics [34]:

$$-r_A = \frac{\partial q}{\partial t} = k_{ads} C_A (q_{max} - q) - k_{des} q \tag{16}$$

Here, k_{ads} is the adsorption rate coefficient, C_A is the concentration in the pore liquid, q_{max} is the maximum adsorption capacity, i.e. the number of binding sites, q is the fraction of occupied binding sites, and k_{des} is the desorption rate coefficient. The kinetic rate parameters have been determined from frontal chromatography experiments [35,36].

2.3.2. Change in pore radius

When molecules bind to the ligands, they will occupy space in the pore, which makes it more difficult for other molecules to diffuse through the pore. q determines how many molecules are bound to the ligands. It is assumed that the protein molecules occupy a layer covering the inner surface of the pore. This method has also been considered by Petropoulos et al. [15]. It underestimates the hindrance, and is thereby most appropriate for high ligand concentrations. This is normally the case for affinity chromatography with a high ligand adsorption capacity at high protein concentration.

The annular volume, V, between two cylinders is given by:

$$V = h\pi(R_{pore}^2 - r^2) \tag{17}$$

and describes the total volume occupied by molecules in a segment of the pore. Thus, the radius changes from R_{pore} to r. The same volume can also be expressed in terms of the molecules that are bound to the ligands within the volume of the segment.

$$V = \left(\frac{4\pi R_0^3}{3}\right) q h \pi R_{pore}^2 A_V \tag{18}$$

Inserting Eq. (17) into Eq. (18) and rearranging gives:

$$r = \left(R_{pore}^2 - \left(\frac{4\pi R_0^3}{3}\right)\frac{q h \pi R_{pore}^2 A_V}{h\pi}\right)^{0.5} \tag{19}$$

Eq. (19) gives the actual pore radius when a certain number of protein molecules have been adsorbed (q).

2.3.3. Determination of q_{max}

The value of q_{max} is normally obtained experimentally as mol adsorbed protein/(m^3 sedimented gel). This must be transformed to mol/(m^3 pore volume), since it is assumed that the adsorbed protein covers the inner surface of the pores.

Through dimensional analysis it can be seen that:

$$\frac{\text{mol}}{\text{m}^3\text{ pores}} = \frac{\text{mol}}{\text{m}^3\text{ sedimented gel}} \frac{\text{m}^3\text{ sedimented gel}}{\text{m}^3\text{ beads}} \frac{\text{m}^3\text{ beads}}{\text{m}^3\text{ pores}}$$

This can also be expressed as Eq. (20) using porosities:

$$q_{\max} = q_{\max\ \text{experimental}} \frac{1}{1-\varepsilon_{\text{bed}}} \frac{1}{\varepsilon_{\text{bead}}} \tag{20}$$

ε_{bed} is the porosity of the packed bed considering the external volume only, i.e. the volume between the beads, and $\varepsilon_{\text{bead}}$ is the porosity inside the gel beads. q is based on the volume of the total pore volume. However, the continuity equation is based on the effective pore volume. Since this decreases as molecules bind to the pore walls this has to be considered in the continuity equation. Thus, another correction factor must be introduced. Relating the effective pore volume to the total pore volume gives:

$$\varepsilon_{\text{r}} = \frac{\text{volume of effective pore volume}}{\text{volume of total pore volume}} = \frac{\pi h r^2}{\pi h R_{\text{pore}}^2} \tag{21}$$

The most realistic approach is to base the number of ligands on the surface area and not on the total gel volume. It is thus assumed that the ligands are evenly distributed over the whole pore surface. Medin [4] has described the pore distribution in a 4% agarose gel. Using his data, it is possible to calculate the ratio between the pore wall surface area and the pore volume, on average, for the whole gel. This ratio, κ_{gel}, was found to be 0.026 nm^{-1}. This is used to transform q from ligands/pore volume to ligands/pore wall surface area. This means that there will be more ligands in the small pores, and fewer in the large pores. However, since the continuity equation uses the pore volume, the value of q must be transformed back to ligands/pore volume for each pore.

$$q_{\max}(R_{\text{pore}}) = q_{\max\ \text{experimental}} \frac{1}{1-\varepsilon_{\text{bed}}} \frac{1}{\varepsilon_{\text{bead}}} \frac{1}{\kappa_{\text{gel}}} \frac{2}{R_{\text{pore}}} \tag{22}$$

2.3.4. Derivation of the largest protein size not filling a pore

Since there are a certain number of ligands in each pore, larger molecules fill a pore faster than smaller molecules. Thus, if the molecule is large enough, radius = $R_{\max}$, the pore will be plugged completely at the entrance and all diffusion into the pore will stop. This happens when the pore radius has decreased to the same size as the molecular radius. This can be derived from Eq. (19) by replacing r with $R_{\max}$ and rearrange:

$$4\frac{\pi}{3} R_{\max}^3 q_{\max} q_{\max\text{Ads}} A_V + \frac{R_{\max}^2}{R_{\text{pore}}^2} - 1 = 0 \tag{23}$$

$q_{\max\text{Ads}}$ is the normalized equilibrium q, i.e. the fraction of $q_{\max}$ that will bind to ligands when in equilibrium with pore concentration. The limiting pore sizes for lysozyme, BSA and IgG are given in Table 3. $q_{\max\text{Ads}}$ is deduced from Eq. (16) when there is no net change in q.

$$q_{\max\text{Ads}} = \frac{k_{\text{ads}} C_{\text{in}}}{k_{\text{ads}} C_{\text{in}} + k_{\text{des}}} \tag{24}$$

Table 3
Number of molecule layers for different molecules and different pore radii at equilibrium when q is based on either volume or surface assumption

Protein	Pore radius				Limiting pore filling radius (nm)
	15 nm		115 nm		
	Volume	Surface	Volume	Surface	
Lysozyme	0.05	0.28	0.40	0.27	3
BSA	0.15	0.92	1.1	0.76	10
IgG	0.28	1.40	2.1	1.4	22

The limiting pore size where the pore is completely filled and thus blocked is also given.

2.4. Extended continuity equation

With a variable diffusion coefficient and a variable porosity the continuity equation is thus deduced to:

$$\frac{\partial C_{\text{A}}}{\partial t} = -\frac{C_{\text{A}}}{\varepsilon_{\text{r}}} \frac{\partial \varepsilon_{\text{r}}}{\partial r} \frac{\partial r}{\partial t} + \frac{D}{\varepsilon_{\text{r}}} \frac{\partial C_{\text{A}}}{\partial z} \frac{\partial \varepsilon_{\text{r}}}{\partial z} + \frac{\partial C_{\text{A}}}{\partial z} \frac{\partial D}{\partial z} + D\frac{\partial^2 C_{\text{A}}}{\partial z^2} + \frac{r_{\text{A}}}{\varepsilon_{\text{r}}} \tag{25}$$

It is derived from a differential mass balance with special consideration to the variable diffusivities and porosities. When the diffusion coefficient and porosity are constant Eq. (25) is shortened to Eq. (2).

2.5. Pore size distribution

As can be seen in Fig. 4, the pore size distribution in agarose gel is bimodal. This can be described by two Gaussian distributions summarized to:

$$f(r) = \sum_{i=1}^{2} \frac{1}{\sigma_i \sqrt{2\pi}} \text{e}^{-(1/2)((r-\mu_i)/\sigma_i)^2} \tag{26}$$

where σ_i is the standard deviation and μ_i is the mean radius of the pores The two Guassian distributions describe the microvoids and pores shown by Medin [4]. Medin used scanning electron microscopy together with image analysis to determine the pore size distribution.

Each distribution is then divided into different classes. When the pores are added together to describe a spherical

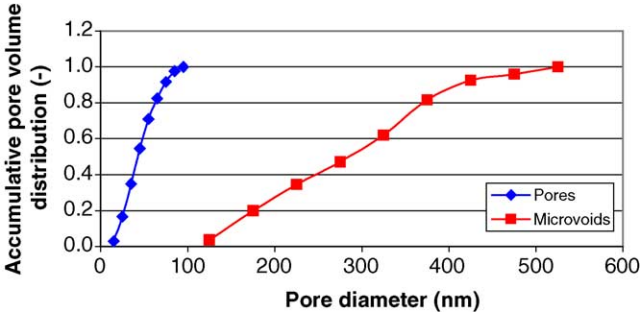

Fig. 4. Accumulative pore volume distribution for pores and microvoids in a 4% agarose gel.

bead, they are scaled with this distribution, but also scaled by the volume, since the volume is larger at the surface than in the center of the beads. This means that there are more pores at the surface, although the porosity and distribution is the same in the whole bead. The scaling procedure is explained in detail in Section 4.4.

3. Materials and methods

3.1. Porous media

When studying diffusion in agarose gels it is very important to know the distribution of the pores. Medin has studied the pore size distribution in 2, 3 and 4% agarose gels [4]. Medin used scanning electron microscopy together with image analysis to determine the pore size distribution. Fig. 4 shows the cumulative pore volume distribution according to Medin's data for a 4% agarose gel. The pores are divided into two classes, pores and microvoids. The range of pore diameters is from 10 to 100 nm, while the range for microvoids is 100–600 nm. In the present work, only a 4% agarose gel has been simulated. However, the model is general and can easily be used to simulate any gel.

3.2. Proteins

To simulate realistic molecules three different molecules have been used: lysozyme, bovine serum albumin (BSA) and immunoglobuline G (IgG). These are well-known proteins and often-used proteins, and it is thus easy to compare results. Some data regarding these molecules can be found in Table 1. The effect of protein charge is not taken into account in the model in order to elucidate the pure effects of adsorption kinetics and diffusion.

3.3. Ligands

The protein molecules bind to different ligands. The following ligands were used in this study: for lysozyme and BSA the ligand Cibacron Blue was used, and for IgG the ligand protein A. However, in some of the comparative simulations, the same adsorption kinetics, as for lysozyme, was used for all three model molecules, to elucidate and analyze the effects of hindered diffusion. In such cases, the ligand was assumed to be Cibacron Blue. Adsorption kinetic parameters are summarized in Table 2.

3.4. Numerical method

The model is described by a parabolic partial differential equation (PDE), Eq. (25), with an associated adsorption kinetic equation, Eq. (16). It is solved by the method of lines based on finite difference approximations of the space dimension, i.e. the pore length. This is discretized into grid points. The approximation results in a large set of ordinary differential equations (ODEs) in time, which are solved with an implicit ODEsolver, in our case ode15s [37]. Base case parameters and protein data used in the simulations are given in Table 2 and Table 1, respectively. Some of the data have been varied in the parameter study to observe the effects of specific parameters.

4. Results

As explained above (Sections 2.3.2–2.3.4) experimentally obtained data for the bound protein must be converted to suit the intrinsic pore model used, i.e. they must be based on pore surface area rather than pore volume. To validate the assumption of using pore surface area instead of pore volume, the two cases are discussed in connection to Table 3 where the thickness of protein layers are given with the different assumptions. When q is based on the pore volume the thickness of the protein layer increases considerably as the pore size increases.

In Table 3, it can be seen that different molecules fill different pores with layers of different thicknesses when q is based on volume. It is assumed that all the ligands are available for binding regardless of the size of the protein molecule. Since the larger molecules occupy more space, they will form thicker layers. When the pore radius increases, the volume of the pore increases, and thus also the number of ligands. The volume density of ligands is constant, but the surface density is different for small and large pores. When the volume of the pore increases the area of the pore also increases. The pore volume increases faster than the pore area as the radius of the pore increases:

$$\frac{\text{pore volume}}{\text{pore area}} = \frac{\pi r^2 L}{\pi 2 r L} = \frac{r}{2} \tag{27}$$

Thus, in a larger pore there will be more layers of molecules. However, the ratio between the original pore radius and the available pore radius at equilibrium is constant, if only the pore radius is changed. Equilibrium is attained more rapidly for a wide pore than for a small pore. This is due to a higher diffusion coefficient in the wider pore. With faster diffusion, the concentration inside the pore will increase faster and the binding kinetics will also increase.

If q is based on surface area instead of volume, the thickness of the protein layer will be almost constant as the pore size increases. The surface density of ligands is constant. However, the protein layer is slightly thicker for smaller pore radii for lysozyme and BSA. This is due to the curvature of the pore. This is, however, not the case for IgG, where the layer is slightly thinner in the small pores. This is because it is impossible for IgG to reach the theoretical equilibrium in the small pores, as they are filled before equilibrium can be reached, due to the high ligand and protein concentration in the present case, see Table 3. In the parameter study below q is based on the surface approximation.

The following parameters were varied in the parameter study.

- Molecule size: lysozyme, BSA and IgG were used.
- Pore radius: 15 and 115 nm were used to describe pores and microvoids, respectively [4].
- Different pore size distributions.

The Renkin diffusion coefficient model has been used throughout the study.

The output data from the simulation program is given in 3Dgraphs showing: diffusion coefficient, pore radius, amount of protein adsorbed and concentration in the pore liquid as a function of time and pore length. A typical 3Dgraph for the diffusion coefficient is shown in Fig. 3. As described in Eqs. (10), (13) and (14) the diffusion coefficient is a function of the molecule and pore radii. Thus, the graphs describing the diffusion coefficient and the graphs describing the pore radius are very similar in shape as a function of time. Although the relationships are not linear with time, the shapes will be very similar. There is also a relation between the bound protein and the pore concentration given by Eq. (16). However, this is also influenced by the diffusion hindrance in the pore. The q–C_A relation is determined by whether the binding is kinetically or mass-transfer controlled.

Figs. 5–10 show how the number of protein molecules bound to the ligands changes with time and porelength, for different molecules and different pore radii. As a basis for comparing the graphs, the time is used at which the end of the pore reaches 80% of the equilibrium value for q for lysozyme. For the microvoids this is achieved after 2.9 h and for the pores after 34.7 h. The various parameters are shown for increasing times from start till the end time as defined above, distributed evenly in time. To study the influence of the diffusive hindrance the same kind of adsorption kinetics was used in all simulations comparing different protein molecules. The same type of gel was also assumed in all simulations. A lower agarose concentration would give larger pores [4] and a higher agarose concentration or a cross-linked gel would give smaller pores [7], which would change all the pore size distributions. Although not discussed in this work, it is important to bear in mind that the gel properties are important for the final result.

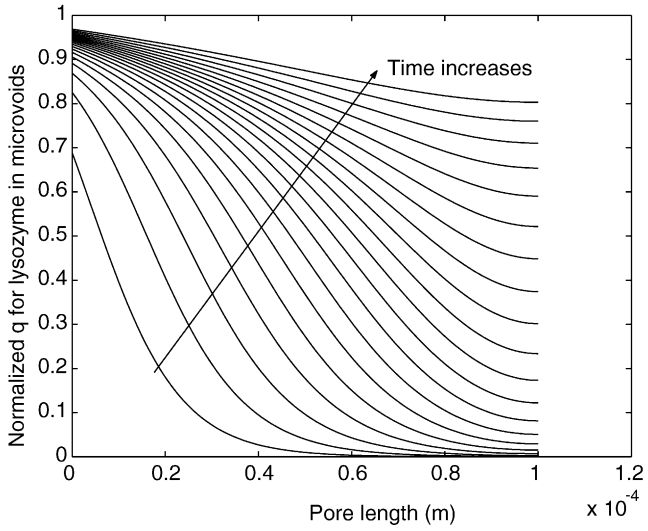

Fig. 5. Normalized q as a function of time and pore length for lysozyme in microvoids. Final time: 2.9 h. The curves are distributed evenly in time between 0 and 2.9 h.

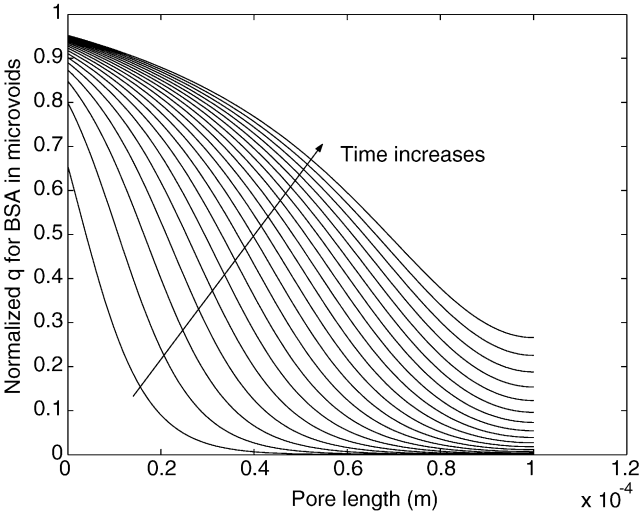

Fig. 6. Normalized q as a function of time and pore length for BSA in microvoids. Final time: 2.9 h. The curves are distributed evenly in time between 0 and 2.9 h.

4.1. Diffusion and adsorption in microvoids

Fig. 5 describes the binding of lysozyme in large microvoids as a function of pore length. The diffusion is not expected to be hindered to any significant degree. Furthermore, when equilibrium is attained there is only a thin layer of molecules on the pore surface, decreasing the pore

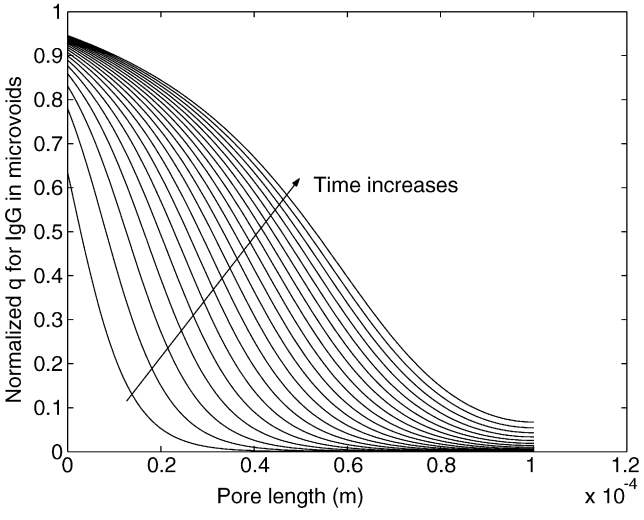

Fig. 7. Normalized q as a function of time and pore length for IgG in microvoids. Final time: 2.9 h. The curves are distributed evenly in time between 0 and 2.9 h.

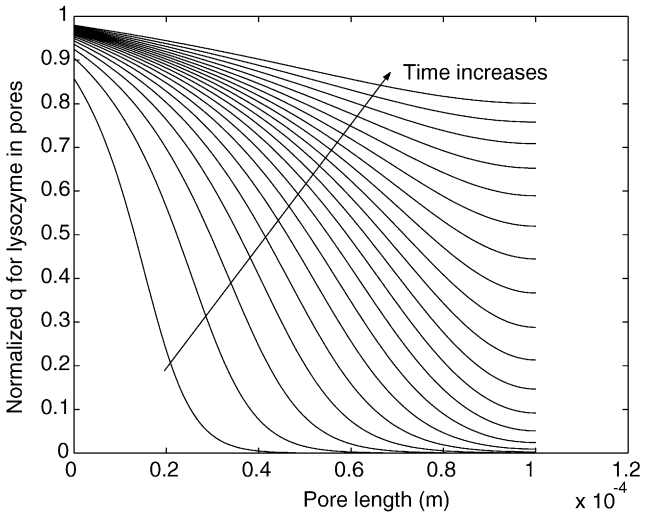

Fig. 8. Normalized q as a function of time and pore length for lysozyme in pores. Final time: 34.7 h. The curves are distributed evenly in time between 0 and 34.7 h.

volume very little, as can be seen in Table 3. q increases steadily until equilibrium is attained. These comparisons were made when the end of the pore had reached 80% of equilibrium for lysozyme. At the starting point no molecules are bound to the ligands, thus q is zero in the whole pore. This is represented by a line following the x-axis. The next curve is, however, higher and q increases continuously with time until equilibrium is attained. At the inlet (pore length = 0), q is above 70% of the equilibrium value because of the high rate of diffusion inside the pore, for the second curve, which is after approximately 8 min.

When using a larger molecule (BSA) the diffusion is slower, although the pore radius does not hinder diffusion much in the large microvoids. This leads to a slower development of the profile. Thus, there will be a steeper gradient for BSA (Fig. 6) compared to lysozyme (Fig. 5). For IgG (Fig. 7) the diffusion is even slower than for BSA. This can be seen at the end of the pore, where q has reached about 10% of the equilibrium value. The different external mass transfer coefficients at the inlet for different proteins affect the inlet concentration.

4.2. Diffusion and adsorption in pores

Figs. 8–10 show the relationships for longer times than in Figs. 5–7. The end time was, however, still defined to be when the lysozyme at the end of the pore had reached 80% of the equilibrium value of q. The longer time was required because the pore was narrower, hindering diffusion considerably. When comparing the adsorption of lysozyme in microvoids with that in pores (Figs. 5 and 8, respectively) the similarity is obvious. However, there are some minor differences. The value of q at the inlet is higher in the pores than in the microvoids, and is more similar to a shrinking core model. The fact that the pores are smaller from the beginning can explain this, and when the molecules bind to the ligands, the narrowing of the pores will obstruct the diffusion further.

In the pores, it is even more noticeable how the differences in diffusion coefficient affect the binding. For BSA (Fig. 9), a rapid decrease in q can be seen. At the end of the pore, q is only a few percent of the equilibrium value.

For IgG (Fig. 10), the hindrance of diffusion by the narrow pores is even more evident. Since the same adsorption kinetics was used to model all molecules these effects must be due to diffusion only. As can be seen, the value of q at the end of the pore is very close to zero. The value of q is also rather small at the entrance. The quotient between the molecule radius and the pore radius is large and thus diffusion is slow. When more molecules bind to the ligands they occupy more space in the

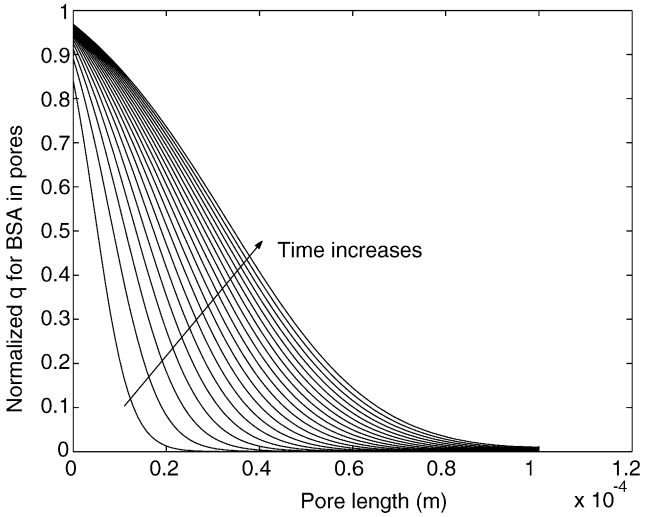

Fig. 9. Normalized q as a function of time and pore length for BSA in pores. Final time: 34.7 h. The curves are distributed evenly in time between 0 and 34.7 h.

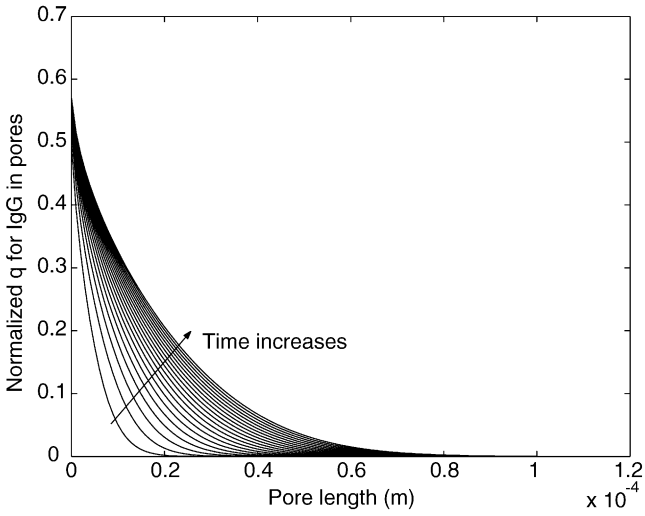

Fig. 10. Normalized q as a function of time and pore length for IgG in pores. Final time: 34.7 h. The curves are distributed evenly in time between 0 and 34.7 h.

pore thereby decreasing the effective pore radius. Eventually, the inlet of the pore will be plugged, preventing any further diffusion. When the pore radius is 15 nm and q_{max} is used, the smallest molecule radius that plugs the pore completely is 3.5 nm. This means that the pore will never attain theoretical equilibrium for IgG since the ligand and protein concentration is high enough to fill the pore, see Table 3. Equilibrium will be obtained for BSA and lysozyme, although this will take a long time for BSA. This explains the low value of bound protein at the inlet, since the pore fill up, and thereby denying access for more protein molecules, and it will take a very long time to fill up all the pore.

4.3. Diffusion and adsorption in different pore size distributions

As has been shown, the diffusion changes considerably with the ratio between molecule and pore radius and this influences the binding of the protein, especially for large protein molecules and small pores. In a gel there is clearly a distribution of pore sizes. Therefore, it will be more difficult to predict the binding when dealing not only with a single pore size (Sections 4.1 and 4.2), but also with a pore size distribution. Figs. 11 and 12 show the distribution of q for microvoids and pores, while Fig. 13 shows that for very narrow pores, 3–8 nm. A curve showing the normal distribution regarding number of pores is also shown in Figs. 11–13.

In the microvoids (Fig. 11), there is no effect of the different molecules. All the protein curves are superimposed due to the very small influence of diffusion hindrance in these large pores at equilibrium. However, this is only true when there is no time dependence. These data were simulated for 1000 h, which is an extremely long time, and should be sufficient to attain steady state. Although the diffusion rate differs, the same steady state will be reached eventually if there is no complete plugging.

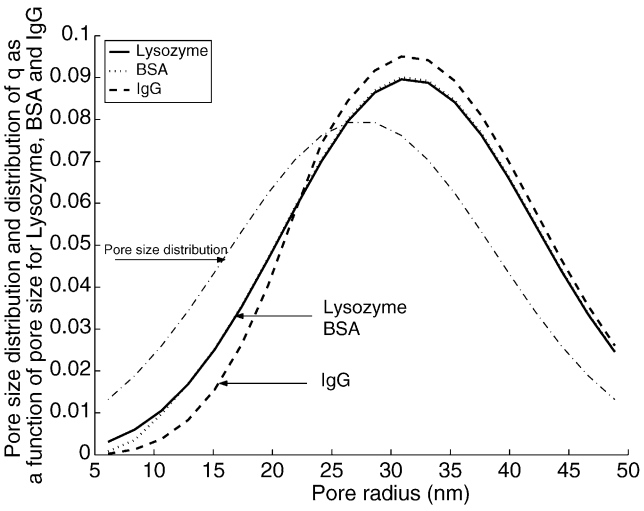

Fig. 12. Distribution of q for different molecules in a normal distributed pore distribution after 1000 h. Gaussian number distribution with μ = 27.5 nm and σ = 11.25 nm.

For the pores (Fig. 12), the curve describing the distribution of IgG is clearly separated from those for lysozyme and BSA. This is due to the smaller pores and the fact that IgG is larger than the other two molecules. Figs. 11–13 show a normalized distribution based on the total amount of protein bound to the ligands. This does not mean, in the pore case (Fig. 12), that more IgG is bound to the ligands, but only that a higher fraction of the protein molecules is bound in the larger pores. This is due to the diffusion restrictions in the small pores. For BSA and lysozyme there is only a difference for the smallest pores.

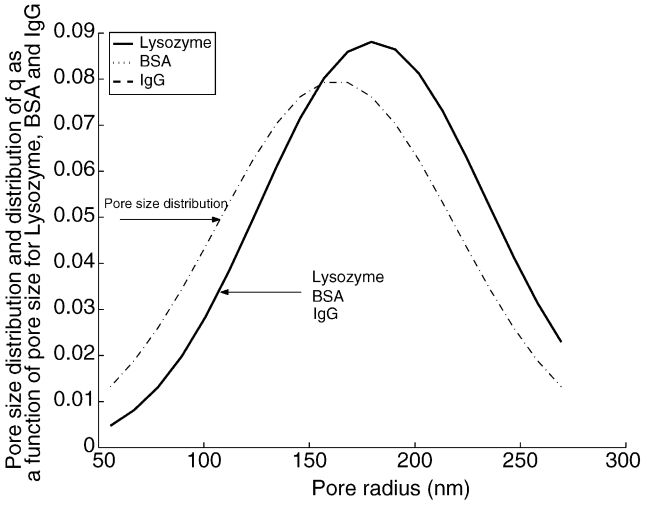

Fig. 11. Distribution of q for different molecules in a normal distributed microvoid distribution after 1000 h. All protein graphs overlap due to the large pore size. Gaussian number distribution with μ = 162.5 nm and σ = 56.25 nm.

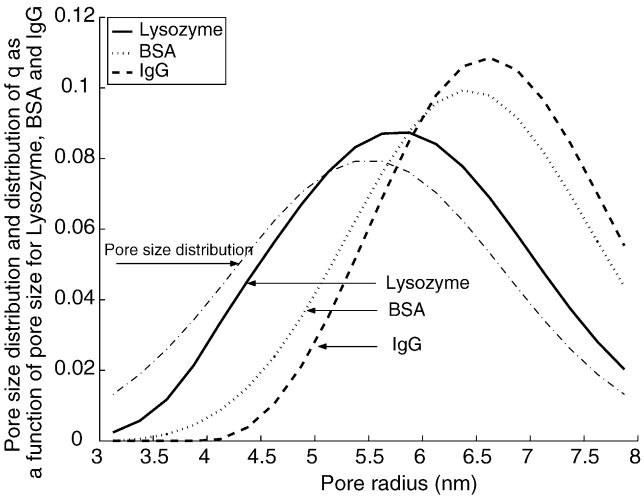

Fig. 13. Distribution of q for different molecules in a normal distributed nanopore distribution after 1000 h. Gaussian number distribution with μ = 5.5 nm and σ = 1.25 nm.

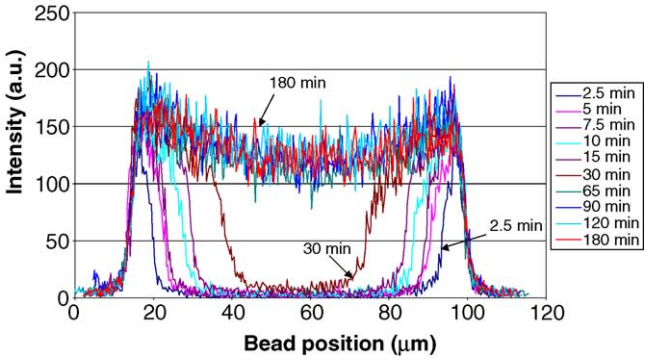

Fig. 14. Intensity profiles of IgG from measurements with confocal microscopy in agarose gel beads. The slight difference in intensity between the center and the surface at final time is due to attenuation although it is minimized using a low fluorophore concentration. (Experimental data is provided by Anders Ljunglöf, Amersham Bioscience, Uppsala.)

4.4. Comparison between simulated data and experimental data from confocal microscopy

It is very difficult to measure the concentration profiles inside gel beads. This can, however, be done by confocal microscopy. Fig. 14 shows the intensity profiles at different times from measurements with confocal microscopy. Original data were kindly supplied by Anders Ljunglöf, Amersham Biosciences, Uppsala [38]. These data were not filtered or normalized, or recalculated to a concentration from intensity. However, since the measurements were performed on different beads, a slight correction for bead size was applied. For comparison, the pore size distribution for cylindrical equally long pores has been converted into spherical geometry by simply scaling by volume. That means that the number of pores decreases towards the center of the bead still having the same size distribution. This results in the simulated concentration profile shown in Fig. 15, which agrees fairly well with the experimental profile shown in Fig. 14, although there is a slight difference in the gels used. Ljunglöf [38] uses a cross-linked gel, while the simulated data are based on Medin's data [4]. To make a more detailed comparison the concentration profiles shown in Figs. 14 and 15 have been integrated to give the total amount of adsorbed protein as a function of time shown in Fig. 16. The difficulty in defining the outer surface of the bead in the confocal measurements and the fluctuating intensity of course makes it difficult to make a thorough comparison. Furthermore, an attenuation effect in the center of the bead at final time underestimates the total amount adsorbed protein slightly. Anyhow, the experimental data shown in Fig. 14 has a slightly more shrinking-core behavior than the simulated data, which is more diffusive in appearance. One explanation to this could be that although the same agarose concentration was used in the confocal and pore-size distribution measurements the confocal data was obtained for a cross-linked commercial gel eventually causing a slightly tighter pore network thereby resulting in a more shrinking-core behavior. Still, remembering that the simple

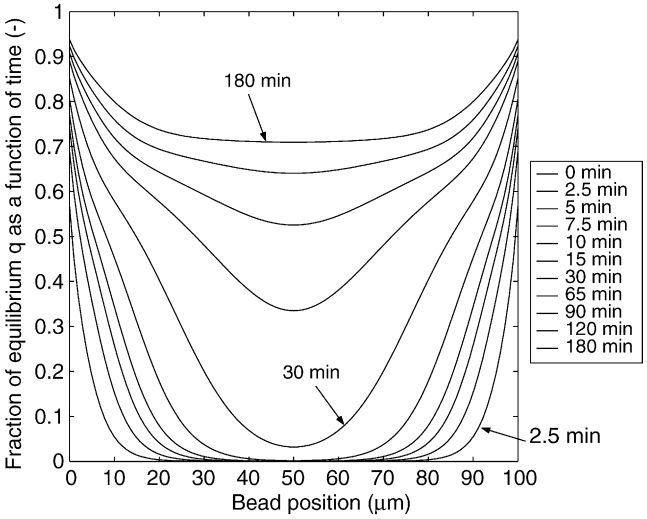

Fig. 15. Simulated data for the fractional approach of q to equilibrium with gel data from Medin [4]. Pores radius vary in size from 10 to 30 nm, and microvoids vary from 50 to 200 nm in radius.

model utilizes no fitting parameters and only our own and other's independent experimental data as input to the simulation model, there is a surprisingly good resemblance between model and experiments. The present simulation shows that confocal adsorption data and simulation models could be used to understand the competing rate processes going on in a chromatographic protein adsorption in a gel. The experimental confocal technique could be refined to increase the resolution even more and to minimize the effects of intensity attenuation especially in the center of the beads. New techniques to determine the pore size distribution in gels in a simple way would be of great value. The simulation models could be improved by using connectivity models although

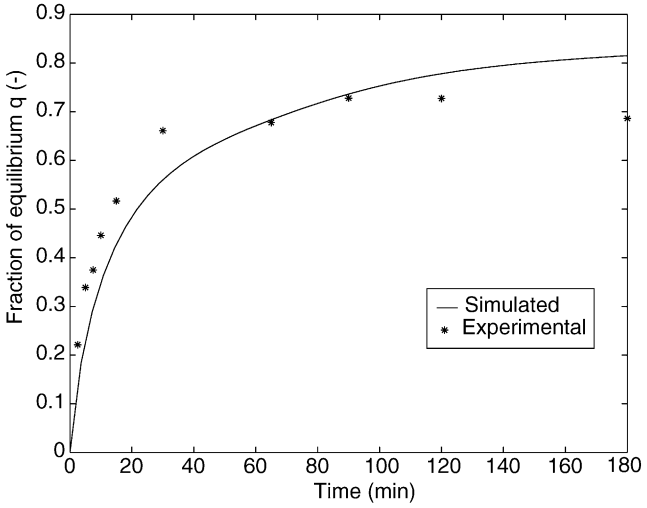

Fig. 16. Comparison between experimental confocal microscopy data and simulated data. An integral value of normalized q for a bead as a function of time. The more shrinking-core behavior for the experimental data in Fig. 14 as compared to simulation data in Fig. 15 is seen in this figure as a slightly faster adsorption for the experimental data.

they would loose in simplicity and would require unknown parameters as fitting parameters. Still, new insights would be gained.

5. Conclusions

In this work, a simulation program has been developed to simulate hindered diffusion of proteins in agarose gels. The model takes into account: (1) different hindered diffusion models, (2) binding kinetics (although the same adsorption kinetics was used in this work to illustrate the effects of diffusion), (3) pore size distributions, (4) external mass transfer outside the agarose beads, and (5) a shrinking effective pore radius due to molecule-to-ligand binding.

The results are presented as 3D and 2D plots giving information on either the fraction of bound molecules, q, the effective diffusion coefficient, D_e, the effective pore radius, r, or the concentration in the pore. Dynamic simulations give the time dependence. The different hindered diffusion models do not differ much within the interesting range. It has been shown how the diffusion is affected by different pore sizes, pore size distributions and also different molecular sizes. Another noticeable effect is the much steeper concentration gradients for the smaller pores compared to the microvoids. These kinds of simulations can be used to find an optimum pore size distribution for the separation of different proteins. In this work, only three protein molecules were considered, but the model can take into account any pore size distribution and any molecule. The present simulation shows that confocal adsorption data and simulation models can be used to understand the competing processes going on in a chromatographic bead during adsorption.

So far, this model only considers diffusion and adsorption of one protein at the time. Thus, there is no competitive adsorption. An extended model is being developed to include also multi component adsorption.

6. Nomenclature

A_V	Avogadro's number (mol^{-1})
C_A	concentration in the pore (mol/m^3)
d_p	bead diameter (m)
D	diffusion coefficient (m^2/s)
D_0	diffusion coefficient in dilute solution (m^2/s)
D_e	effective diffusion coefficient (m^2/s)
f	pore size distribution function
h	length of a segment in the pore (m)
k_{ads}	adsorption rate coefficient ($m^3/(mol\,s)$)
k_B	Boltzmann's constant (J/K)
k_{des}	desorption rate coefficient (s^{-1})
K_{mass}	external mass transfer coefficient (m/s)
L	length of pore (m)
MW	molecular weight (g/mol)
q	amount of bound ligands ($mol/(m^3$ pore))
q_{max}	total amount of ligands ($mol/(m^3$ pore))
$q_{max\ experimental}$	total amount of ligands ($mol/(m^3$ sedimented gel))
q_{maxAds}	value of q at which equilibrium is reached
r	effective pore radius (m)
r_A	rate of adsorption/desorption ($mol/(m^3$ pore s))
R	universal gas constant (J/(K mol))
R_0	molecular radius (m)
Re	Reynolds number (–)
R_{max}	limiting value of R_0 plugging the pore (m)
R_{pore}	pore radius (m)
Sc	Schmidt number (–)
Sh	Sherwood number (–)
t	time (s)
T	temperature (K)
V_{sup}	superficial bulk velocity (m/s)
z	length coordinate of pore (m)

Greek letters

ε	porosity
ε_{bead}	porosity of the bead
ε_{bed}	porosity of the bed
ε_r	shrinking pore coefficient (actual pore volume/total pore volume) (–)
κ_{gel}	specific surface area; the pore wall surface area/pore volume (m^{-1})
λ	ratio between molecule radius and pore radius (–)
μ	dynamic viscosity (Pa s)
μ_i	mean pore radius of distribution i (m)
ρ	density of molecule (kg/m^3)
σ_i	standard deviation (m)

Acknowledgements

The Swedish Centre for BioSeparation is gratefully acknowledged for financial support. Anders Ljunglöf, Amersham Biosciences, Uppsala, is gratefully acknowledged for supplying original confocal data from his work [38].

References

[1] J. Gutenwik, B. Nilsson, A. Axelsson, Biotechnol. Bioeng. 79 (2002) 664.
[2] T. Ehtezazi, C. Washington, J. Control. Release 68 (2000) 361.
[3] J.A. Wesselingh, J. Control. Release 24 (1993) 47.
[4] A. Medin, Studies on Structures and Properties of Agarose, Uppsala University, Uppsala, Sweden, 1995.
[5] K.C. Loh, D.I.C. Wang, J. Chromatogr. A 718 (1995) 239.
[6] C.L. Chiang, T.C. Wu, Y.J. Wang, Biotechnol. Bioeng. 35 (1990) 976.
[7] R.H. Li, D.H. Altreuter, F.T. Gentile, Biotechnol. Bioeng. 50 (1996) 365.
[8] M.A. McCoy, A.I. Liapis, J. Chromatogr. 548 (1991) 25.
[9] D.S. Clark, J.E. Bailey, D.D. Do, Biotechnol. Bioeng. 27 (1985) 208.
[10] L.M. Bryntesson, J. Chromatogr. A 945 (2002) 103.

[11] J.J. Meyers, A.I. Liapis, J. Chromatogr. A 827 (1998) 197.
[12] J.J. Meyers, A.I. Liapis, J. Chromatogr. A 852 (1999) 3.
[13] J.J. Meyers, O.K. Crosser, A.I. Liapis, J. Biochem. Biophys. Methods 49 (2001) 123.
[14] J.J. Meyers, O.K. Crosser, A.I. Liapis, J. Chromatogr. A 908 (2001) 35.
[15] J.H. Petropoulos, A.I. Liapis, N.P. Kolliopoulos, J.K. Petrou, N.K. Kanellopoulos, Bioseparation 1 (1990) 69.
[16] L. Zhang, N.A. Seaton, AIChE J. 38 (1992) 1816.
[17] S. Reyes, K.F. Jensen, Chem. Eng. Sci. 40 (1985) 1723.
[18] R.B. Bird, W.E. Stewart, E.N. Lightfoot, Transport Phenomena, Wiley, New York, 2002.
[19] J. Crank, The Mathematics of Diffusion, Oxford University Press, Oxford, 1975.
[20] E.L. Cussler, Diffusion, Mass Transfer in Fluid Systems, Cambridge University Press, Cambridge, 1997.
[21] S. Kou, Transport Phenomena and Materials Processing, Wiley, 1996.
[22] R.L. Fournier, Basic Transport Phenomena in Biomedical Engineering, Taylor & Francis, 1999 (Chapter 2).
[23] H. Brenner, L.J. Gaydos, J. Colloid Interface Sci. 58 (1977) 312.
[24] E.M. Renkin, J. Gen. Physiol. 38 (1954) 225.
[25] B.A. Westrin, Diffusion measurements in gels. A methodological study, Chemical Engineering, Lund University, Lund, Sweden, 1991.
[26] A.G. Ogston, B.N. Preston, J.D. Wells, Proc. R. Soc. London A333 (1973) 297.
[27] M. Moussaoui, M. Benlyas, P. Wahl, J. Chromatogr. 591 (1992) 115.
[28] C. Mattisson. Diffusion studies in gels using holographic laser interferometry, Chemical Engineering, vol. 1, Lund University, Lund, Sweden, 1999.
[29] L. Masaro, X.X. Zhu, Prog. Polym. Sci. 24 (1999) 731.
[30] P.M. Boyer, J.T. Hsu, AIChE J. 38 (1992) 259.
[31] J.C. Bosma, J.A. Wesselingh, J. Chromatogr. B 743 (2000) 169.
[32] H. Faxén, Ark. Mater. Astron. Fys. 17 (1923) 1.
[33] J.D. Ferry, J. Gen. Physiol. 20 (1936) 95.
[34] F. Carlsson, Mathematical modelling and simulation of fixed-bed chromatographic processes, Chemical Engineering, vol. 1, Lund University, Lund, Sweden, 1994.
[35] P. Persson, H. Kempe, G. Zacchi, B. Nilsson, Process Biochem. (2004) in press.
[36] H. Kempe, A. Axelsson, B. Nilsson, G. Zacchi, J. Chromatogr. A 846 (1999) 1.
[37] M.E. Davis, Numerical Methods and Modeling for Chemical Engineers, Wiley, New York, 1984.
[38] A. Ljunglöf, Direct observation of biomolecule adsorption and spatial distribution of functional groups in chromatographic adsorbent particles, Center for Surface Biotechnology, Uppsala, Sweden, 2002.